# Realizing Unitary k-designs with a Single Quench

Yi-Neng Zhou,\* Robin Löwenberg, and Julian Sonner<sup>†</sup> Department of Theoretical Physics, University of Geneva, 24 quai Ernest-Ansermet, 1211 Genève 4, Suisse

We present a single-quench protocol that generates unitary k-designs with minimal control. A system first evolves under a random Hamiltonian  $H_1$ ; at a switch time  $t_s \geq t_{\rm Th}$  (the Thouless time), it is quenched to an independently drawn  $H_2$  from the same ensemble and then evolves under  $H_2$ . This single quench breaks residual spectral correlations that prevent strictly time-independent chaotic dynamics from forming higher-order designs. The resulting ensemble approaches a unitary k-design using only a single control operation—far simpler than Brownian schemes with continuously randomized couplings or protocols that apply random quenches at short time intervals. Beyond offering a direct route to Haar-like randomness, the protocol yields an operational, measurement-friendly definition of  $t_{\rm Th}$  and provides a quantitative diagnostic of chaoticity. It further enables symmetry-resolved and open-system extensions, circuit-level single-quench analogs, and immediate applications to randomized measurements, benchmarking, and tomography.

Introduction— Random unitaries play a central role in quantum chaos and thermalization [1–4], quantum computation [5], quantum state tomography [6–9], and quantum cryptography [10]. In quantum computing, Haar-random unitaries underpin randomized benchmarking [11, 12] and randomized measurements [8, 13–17] and also serve as a resource for demonstrations of quantum-advantage [18–20]. In many-body dynamics, scrambling and the emergence of Haar-like behavior provide tractable models for chaotic systems and illuminate their spectral statistics and dynamical properties. The Haar measure further enables analytic control through its symmetries and deep connections to random-matrix theory (RMT) [21–25].

Given these broad applications — and because exact sampling from the Haar measure is prohibitively expensive [26] — a central challenge is to generate ensembles that realize unitary k-designs [27-33]. A unitary k-design is an ensemble whose moments match those of the Haar measure up to order k and is a key benchmark of Haar randomness. The goal, therefore, is to realize unitary k-designs with minimal experimental control overhead. Much progress has come from circuit implementations, but these either require finely structured gate sequences or rapidly varying random interactions—both of which depart from natural Hamiltonian evolution [34-39]. By contrast, Hamiltonian dynamics, particularly with time-independent couplings, offer a more practical route for experiments.

Quantum chaotic systems scramble information: localized information rapidly delocalizes and mixes, suggesting a quantitative link between chaos and Haar randomness [1, 2, 4, 37, 40-44]. This motivates using chaotic dynamics to approximate Haar statistics. However, purely time-independent chaotic evolution typically fails to reproduce Haar moments beyond low orders [1, 45, 46]. By contrast, Brownian (continuously randomized) evolutions can reach k-designs on time/depth poly in k and system size, but at the cost of rapid, sustained modula-

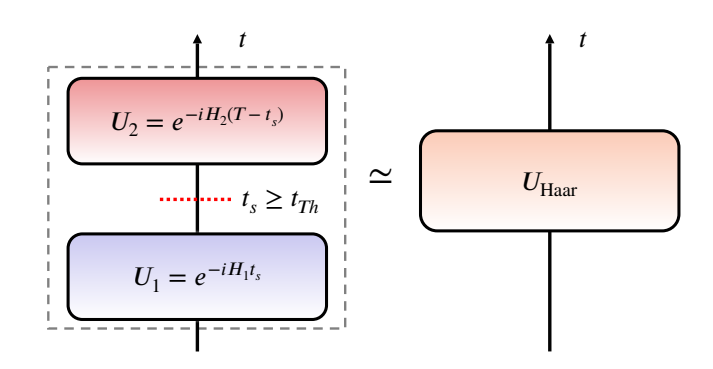
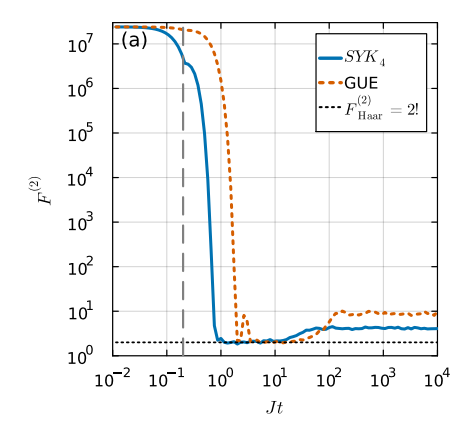
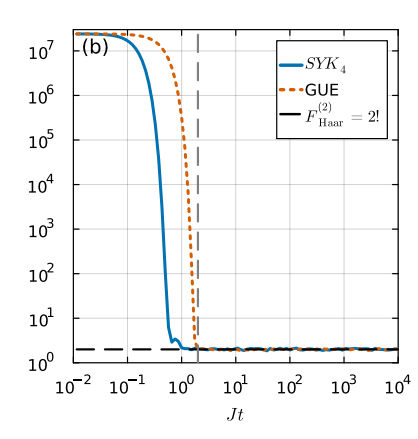


FIG. 1. Single-quench protocol for generating unitary k-designs. The system evolves under  $H_1$  for  $0 < t \le t_s$ . At the switch time  $t = t_s$ , a sudden quench changes the Hamiltonian to  $H_2$ , under which it evolves for  $t_s < t \le T$ . Despite requiring only one control action, the protocol retains the design-forming power of Brownian schemes and realizes a unitary k-design when  $t_s \ge t_{\text{Th}}$  (the Thouless time).

tion of couplings that is difficult to implement experimentally [38, 42, 45, 47–49]. These considerations motivate the search for efficient, experimentally viable Hamiltonian protocols that achieve unitary designs with minimal control.

In this Letter, we introduce a single-quench random-Hamiltonian evolution that realizes unitary k-designs with minimal control. The system first evolves under a random Hamiltonian  $H_1$ ; at a chosen switch time  $t_s$ , it is quenched to an independent random Hamiltonian  $H_2$  sampled from the same ensemble, and then the system evolves under  $H_2$ . This single quench disrupts residual spectral and structural correlations that otherwise obstruct design formation, and we show that for  $t_s \geq t_{\rm Th}$  (the Thouless time) the resulting ensemble attains the unitary k-design benchmarks. Despite requiring only one control action, the protocol retains the design-forming power of Brownian schemes. We fur-





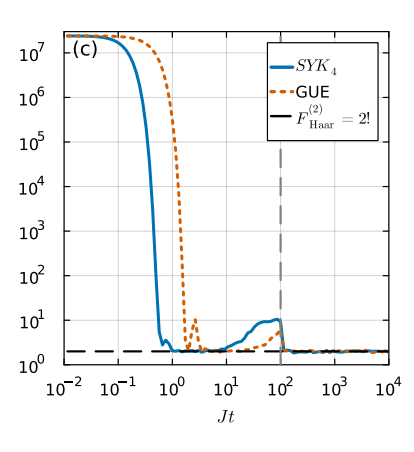


FIG. 2. Second-order frame potential  $F^{(2)}$  versus total evolution time for single-quench dynamics of the complex-fermion SYK4 in a fixed charge sector (blue solid) and the GUE random-matrix ensemble (red dashed). Parameters: SYK—N=8, q=4, J=1; GUE—Hilbert-space dimension  $N_{\rm dim}=70$ . Curves are averages over 4000 disorder realizations. The Haar benchmark  $F^{(2)}=2$  is shown as a black dotted line. Gray dashed vertical lines mark the switch time  $t_s$  in each panel: (a)  $Jt_s=0.2$  (before the Thouless time  $t_{\rm Th}$ ), (b)  $Jt_s=2.0$  (near  $t_{\rm Th}$ ), and (c)  $Jt_s=100.0$  (after  $t_{\rm Th}$ ). At late times, the  $F^{(2)}$  plateau lies above the Haar value for  $t_s< t_{\rm Th}$  and saturates the Haar value for  $t_s> t_{\rm Th}$ .

ther analyze multi-quench evolution that systematically reduces the design error and achieves a target accuracy  $\varepsilon$  with only  $O(\log(1/\varepsilon))$  quenches. The approach applies broadly across chaotic platforms (e.g., trapped ions, superconducting qubits, cold atoms), providing a practical route to scalable unitary designs. Finally, the proximity of the single-quench ensemble to Haar randomness yields an operational definition of Thouless time [50–55] and a quantitative diagnostic of chaoticity.

Single-quench evolution protocol— Consider a system with a random Hamiltonian, e.g., a random matrix sampled from the GUE or a model with random couplings. In the single-quench protocol, the Hamiltonian is

$$H(t) = \begin{cases} H_1, & 0 \le t < t_s, \\ H_2, & t \ge t_s, \end{cases}$$
 (1)

where  $H_1$  and  $H_2$  are independent draws from the same random ensemble. In this protocol, we quench the Hamiltonian from  $H_1$  to  $H_2$  at time  $t_s$ . The time-evolution operator is therefore

$$U(t;t_s) = \begin{cases} e^{-iH_1t}, & 0 \le t \le t_s, \\ e^{-iH_2(t-t_s)} e^{-iH_1t_s}, & t > t_s. \end{cases}$$
 (2)

Here,  $U(t;t_s)$  denotes the total evolution up to time t, with a single quench occurring at time  $t_s$ . This single-quench evolution protocol is illustrated in Fig. 1.

To certify that the single-quench evolution of chaotic models can realize a unitary k-design, we need to quantify the deviation of an ensemble from the Haar random ensemble. This can be done via the frame potential. For an ensemble  $\nu \subset U(d)$ , its k-th order frame potential (FP) [1, 2, 33, 56–58] is defined as

$$F_{\nu}^{(k)} = \mathbb{E}_{U,V \sim \nu} \left| \text{Tr}(U^{\dagger}V) \right|^{2k}, \ k \in \mathbb{N}.$$
 (3)

Among all the random unitary ensembles, the Haar random ensemble minimizes the FP:

$$F_{\nu}^{(k)} \ge F_{\text{Haar}}^{(k)} = k! \text{ for } d \ge k,$$
 (4)

with equality iff  $\nu$  is a unitary k-design. Thus, the gap

$$\Delta_{\nu}^{(k)} = F_{\nu}^{(k)} - F_{\text{Haar}}^{(k)} \tag{5}$$

provides a convenient scalar measure of "distance" to Haar;  $\Delta^{(k)}=0$  certifies a unitary k-design.

Single-quench chaotic evolution realizes unitary design— We simulate the single-quench evolution in two chaotic ensembles—the complex-fermion Sachdev-Ye-Kitaev (SYK) model [59–73] (Fig. 2 as blue solid lines) and Gaussian Unitary Ensemble (GUE) random matrices (Fig. 2 as red dotted lines)—and evaluate the FP as a function of time. For the SYK model, we consider a quantum system composed of complex fermions with all-to-all interaction, whose Hamiltonian is

$$H_{\text{SYK}} = \sum_{1 \le i < j < k < l \le N} J_{ijkl} c_i^{\dagger} c_j^{\dagger} c_k c_l, \tag{6}$$

where  $c_i(c_i^{\dagger})$  denotes the annihilation(creation) operator of complex fermions that satisfies the anticommutation relation  $\{c_i, c_j^{\dagger}\} = \delta_{ij}$ . Here,  $J_{ijkl}$  is a Gaussian random variable with zero mean and variance

$$\langle J_{ijkl}J_{i'j'k'l'}\rangle = \delta_{i,i'}\delta_{j,j'}\delta_{k,k'}\delta_{l,l'}\frac{3!J^2}{N^3}.$$

In both cases, when the switch time  $t_s$  is at or beyond the Thouless time  $t_{\rm Th}$ , its k-th FP saturates the Haar value, indicating that the protocol realizes a unitary k-design (see Fig. 2(b),(c) for k=2). For  $t_s < t_{\rm Th}$ , the late-time plateau lies above the Haar value (see Fig. 2(a)), so a unitary k-design is not achieved.

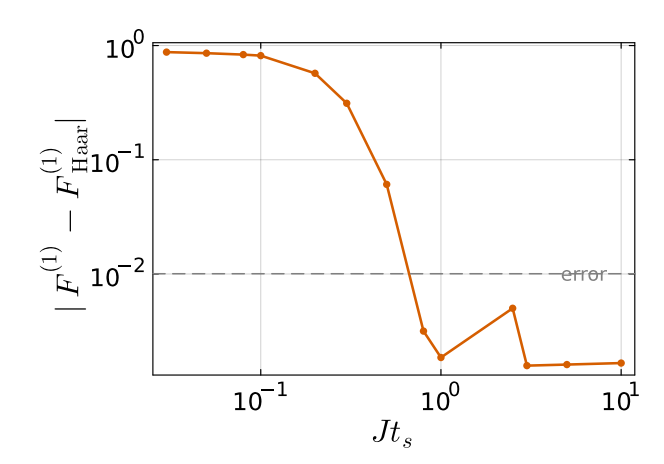


FIG. 3. Gap  $\Delta_{\rm FP}(t_s)$  between the late-time plateau of the first-order frame potential  $F^{(1)}$  and its Haar value for singlequench evolution of the complex SYK<sub>4</sub> model in a fixed charge sector, plotted versus the switch time  $t_s$ . Parameters: N=6, total charge q = 2, J = 1; averaged over  $N_{\rm rand} = 10^4$  disorder realizations. The Thouless time  $t_{\rm Th}$  is defined as the first  $t_s$ at which  $\Delta_{\text{FP}}(t_s)$  is consistent with zero within the statistical uncertainty (gray dashed line). The uncertainty is estimated as  $\sqrt{1/[\sqrt{N_{\mathrm{rand}}}(\sqrt{N_{\mathrm{rand}}}-1)]} \simeq 0.01$ .

As  $t_s$  approaches  $t_{\rm Th}$  from below, the gap  $\Delta_{\rm FP}(t_s)$  between the late-time plateau and the Haar value decreases monotonically. Plotting  $\Delta_{\rm FP}(t_s)$  versus  $t_s$  shows that it approaches zero and then remains small and nearly flat for  $t_s \gtrsim t_{\rm Th}$ , as illustrated in Fig. 3 for the single-quench time evolution of the complex SYK model. This behavior motivates an operational definition of the Thouless time:

$$t_{\rm Th} := \min\{t_s : \Delta_{\rm FP}(t_s) \text{ decreases to zero}$$
(within statistical uncertainty)\}. (7)

Unlike the SFF-based definition that relies on identifying the onset of the linear ramp—often obscured by intrinsic oscillations—our criterion is less ambiguous because the decaying SFF envelope suppresses these oscillations [74].

The single-quench protocol reaches a unitary design on the Thouless-time scale of the underlying dynamics. In strongly chaotic models, one expects this Thouless time to be as short as possible. For example, the SYK model has been argued to have a Thouless time of order  $\sqrt{N \log N}$  in a supersymmetric sigma model approach [75, 76]. It would be interesting to investigate whether a certain class of models might exhibit a fastergodic behavior[77], analogous to the fast-scrambling In contrast, for an integrable random behavior[78]. Hamiltonian—such as the complex SYK<sub>2</sub> model—the same single-quench protocol fails to generate higher-order unitary k-designs. Thus, realizability within this protocol could serve as an operational diagnostic of quantum chaos. Figure 4 plots the FP  $F^{(k)}$  for k = 1, 2, 3, 4 versus total evolution time t for (a) the chaotic complex  $SYK_4$ model and (b) the integrable complex SYK<sub>2</sub> model. In

SYK<sub>4</sub>,  $F^{(k)}$  saturates the Haar benchmarks  $F_{\text{Haar}}^{(k)} = k!$  up to k = 4, demonstrating unitary k-design behavior through fourth order, whereas SYK2 reaches only the k = 1 (unitary 1-design) value [79]. Additional results, including SYK2 and the Richardson model (both interacting and integrable), are presented in the supplementary material (SM) [80].

Random matrix analysis.— We next analyze the singlequench evolution with Hamiltonians sampled from the GUE using RMT analysis, focusing on the first-order FP as a simple, explicit example. We will show that the term controlling the FP-Haar deviation vanishes in the thermodynamic limit once the switch time exceeds the Thouless time. This term is expressed directly via the SFF, making the "FP-Haar gap" definition of the Thouless time equivalent to the standard definition based on the onset of the SFF linear ramp.

For reference, the first-order FP for the unitary time evolution generated from GUE is written as

$$F^{(1)}(t) = \int dH_1 dH_2 P(H_1) P(H_2) \left| \text{Tr} \left( e^{iH_1 t} e^{-iH_2 t} \right) \right|^2.$$
(8)

Here,  $P(H_i) = e^{-\frac{d}{2} \text{Tr}(H_i^2)}$ .

For the single-quench of total evolution time t and switch H at time  $t_s$ , its first-order FP is

$$F^{(1)}(t;t_s) = \int \left( \prod_{a=1}^4 dH_a P(H_a) \right) \times \left| \text{Tr} \left( e^{iH_1(t-t_s)} e^{iH_2 t_s} e^{-iH_3 t_s} e^{-iH_4(t-t_s)} \right) \right|^2,$$
(9)

with  $H_1,H_2,H_3,H_4$  i.i.d. GUE. Write  $e^{iH_at}=V_a\Lambda^aV_a^\dagger$  ( $\Lambda^a$  is diagonal), and use the unitary-conjugation invariance of the GUE measure. Defining  $U^4 := (U^1 U^2 U^3)^{\dagger}$  and  $U^a := V_a^{\dagger} V_{a+1} (a = 0)^{\dagger}$ 1, 2, 3), one obtains

$$F^{(1)}(t;t_s) = \int \left(\prod_{a=1}^4 D\lambda_a\right) \int_{\text{Haar}} dU^1 dU^2 dU^3$$

$$\left| \text{Tr} \left(\Lambda^{1\dagger} U^1 \Lambda^{2\dagger} U^2 \Lambda^3 U^3 \Lambda^4 U^4 \right) \right|^2.$$
(10)

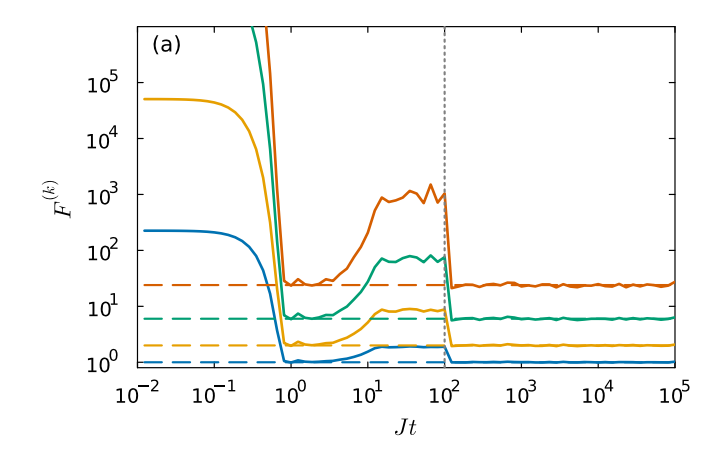
Performing the Haar integrals over  $U^1, U^2, U^3$  using second-moment Weingarten calculus, the leading contribution at large Hilbert-space dimension d is

$$F^{(1)}(t;t_s) = 1 + d^2 \left(\frac{R_2(t-t_s)}{d^2}\right)^2 \left(\frac{R_2(t_s)}{d^2}\right)^2 + \mathcal{O}\left(d^{-1}\right).$$
(11)

Here  $R_2(t) = \int D\lambda \sum_{i,j} e^{i(\lambda_i - \lambda_j)t}$  is the spectral form factor (SFF). For GUE, one may write

$$R_2(t) = d + d^2 r_1^2(t) + d r_2(t), (12)$$

where  $r_1(t)$  and  $r_2(t)$  encode the familiar dip-rampplateau structure [2] (their explicit forms are not needed



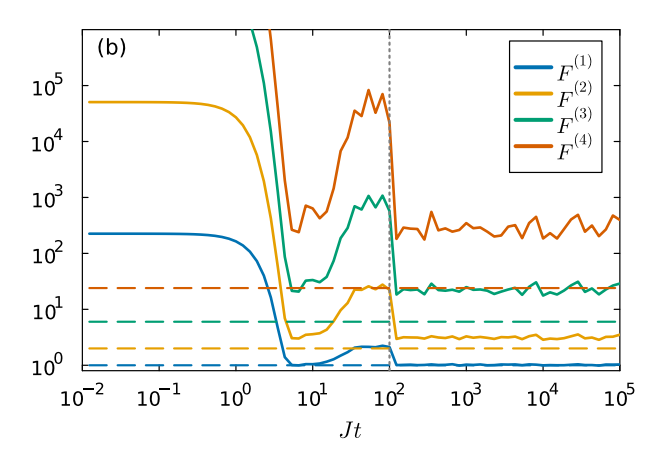


FIG. 4. Frame potentials  $F^{(k)}$  for orders k=1,2,3,4 versus total evolution time Jt under the single-quench evolution in (a) complex SYK<sub>4</sub> model and (b) complex SYK<sub>2</sub> model. Curves for k=1,2,3,4 are shown in blue, orange, green, and vermilion, respectively; the Haar benchmarks  $F^{(k)}_{\text{Haar}} = k!$  appear as dashed lines of matching colors. The gray dotted vertical line marks the switch time  $Jt_s = 100$ . Parameters: N=6 complex fermions in fixed-charge sector q=2, J=1; averages over  $10^4$  disorder realizations. In (a), SYK<sub>4</sub> saturates the Haar values up to k=4, whereas in (b), SYK<sub>2</sub> achieves only the k=1 (unitary 1-design) benchmark.

below). Equation (11) reduces to the single evolution (without single quench) result at  $t-t_s=0$ . At the dip (Thouless) time  $t_{\rm Th}$ ,  $R_2(t_s)\sim \sqrt{d}$ ; on the plateau,  $R_2(t_s)\sim d$ . Hence, if the switch time satisfies  $t_s\geq t_{\rm Th}$ , the second term in (11) vanishes in the thermodynamic limit  $d\to\infty$ . Consequently,  $F^{(1)}(t;t_s)\to 1$ , the Haar value of the first-order FP.

Intuitively, replacing a single uninterrupted evolution with a single quench factorizes the deviation from the Haar average into two SFF-controlled factors, one from the segment of length  $t_s$  and one from the segment of length  $t-t_s$ . The SFF contribution from the first segment decays from t = 0 to the dip and becomes parametrically small once  $t_s \gtrsim t_{\rm Th}$ ; multiplying by this small factor suppresses the overall deviation to  $\mathcal{O}(1/d^2)$ , which vanishes as  $d \to \infty$ . Without the quench, this extra suppression is absent, so the long-time deviation remains set by the late-time SFF and is  $\mathcal{O}(1)$ . In particular, the deviation from the unitary 1-design value is bounded by  $\mathcal{O}(1/d^2)$ : in the large Hilbert space limit, this single-quench protocol realizes an exact unitary 1-design, while for finite d it achieves an approximate 1-design with relative error  $\mathcal{O}(1/d^2)$ . Multiple quenches further reduce this error.

The same structure persists for higher-order frame potentials: the deviation from the Haar value is a product of higher-order SFF factors and vanishes in the thermodynamic limit once  $t_s > t_{\rm Th}$ . Therefore, locating  $t_{\rm Th}$  via the closing of the FP-Haar gap is equivalent to identifying the onset of the SFF's linear ramp, providing an operational—and experimentally convenient—definition of the Thouless time.

One may ask whether the convergence to a k-design could be improved even further by re-sampling m times during the protocol. For an quench m-time (m > 1) FP,

the leading order contribution is

$$F_m^{(1)}(t_1, t_2, ..., t_{m+1}) = 1 + d^2 \prod_{j=1}^{m+1} \left(\frac{R_2(t_j)}{d^2}\right)^2 + \mathcal{O}\left(d^{-1}\right).$$
(13)

Here,  $F_m^{(1)}(t_1, t_2, \dots, t_{m+1})$  denotes the case where the j-th quench is performed at time  $t = \sum_{r=1}^{j} t_r$ . If we assume each time segment is the same, then we have

$$F_m^{(1)}(\Delta t, \dots, \Delta t) = 1 + d^2 \left(\frac{R_2(\Delta t)}{d^2}\right)^{2(m+1)} + \mathcal{O}\left(d^{-1}\right).$$
(14)

Thus, by fixing a small time step  $\Delta t$  and evaluating its SFF, we can compute the corresponding correction using Eq. (11). If we aim to realize a unitary 1-design with error smaller than  $\epsilon$ , Eq. (14) implies that the quench time must satisfy

$$m > \frac{\log(d^2/\epsilon)}{2\log(d^2/R_2(\Delta t))} - 1. \tag{15}$$

Approximate k-designs via multiple-quench— In realistic settings, one only needs to reach a unitary k-design up to a relative error  $\epsilon$ . We say an ensemble  $\nu$  on U(d) is an Tensor Product Expander (TPE)  $\epsilon$ -approximate unitary k-design [35, 37, 81–85] if and only if

$$\left\| \mathbb{E}_{V \sim \varepsilon} \left[ V^{\otimes k} \otimes V^{* \otimes k} \right] - \mathbb{E}_{U \sim \mu_H} \left[ U^{\otimes k} \otimes U^{* \otimes k} \right] \right\|_{\infty} \le \epsilon.$$
(16)

Using the amplification property of TPE [85]: for  $1 \ge \epsilon_0 \ge \epsilon > 0$ , if a unitary ensemble  $\nu$  is a TPE  $\epsilon_0$ -approximate k-design, then the ensemble  $\nu_P$  of products

$$U_P \cdots U_1, \qquad U_j \sim \nu \text{ i.i.d.},$$
 (17)

is an  $\epsilon$ -approximate k-design where P is a positive integer such that  $P \geq \frac{\log(1/\epsilon)}{\log(1/\epsilon_0)}$ . Thus, one can use the multiple-quench protocol to reach an approximate k-design. For a single-quench evolution of total time  $\Delta t$  that reaches a  $\epsilon_0$ -approximate k-design, one can quench the evolution every  $\Delta t$  interval for M time to achieve an  $\epsilon$ -approximate k-design, and we only need

$$M \ge \frac{\log(1/\epsilon)}{\log(1/\epsilon_0)} - 1. \tag{18}$$

The number of quench and also the total evolution time, which is  $T = (M+1)\Delta t$ , grow only logarithmically with the target accuracy, a favorable scaling for experiments. A proof of this amplification of the relative error for the unitary k-design is included in the SM [80].

Conclusion and discussion— In this letter, we show that a *single-quench* evolution of a quantum-chaotic system can realize unitary k-designs. Leveraging fast scrambling, chaotic dynamics serve as efficient randomness generators: unlike strictly time-independent chaotic Hamiltonians—which typically fail beyond low moments—the single-quench protocol attains Haar-level frame potentials once the switch time  $t_s$  reaches the Thouless time  $t_{\rm Th}$ . In contrast to Brownian (continuously randomized) schemes that require rapid, persistent modulation of couplings, our protocol uses only one quench, greatly simplifying implementation[86]. Moreover, in the more realistic setting where we aim to realize approximate unitary kdesigns with relative error  $\epsilon$ , a multiple-quench protocol can be used to reduce the error. The required number of quenches is proportional to  $\log(1/\epsilon)$ .

Beyond providing a simple route to Haar-like randomness, the protocol yields an operational definition of the Thouless time:  $t_{\rm Th}$  is the smallest switch time  $t_s$  after which the late-time frame-potential gap to Haar vanishes within statistical uncertainty. This agrees with the spectral criterion (onset of the ramp in the SFF) while offering an experiment-friendly measurement procedure. Moreover, the single-quench realizability furnishes a quantitative diagnostic of the underlying model's chaoticity.

Our finding—that a single quench suffices to realize unitary k-designs—opens several concrete directions: (i) Integrability and weak chaos: How effective is the single-quench protocol in the integrable or near-integrable regime? Does it reproduce the Brownian dynamics of the model? Can the approach to a k-design serve as a quantitative diagnostic of chaos as integrability is tuned? (ii) Minimal perturbations: Replacing the quench with a weak random perturbation of a time-independent Hamiltonian may provide an even lighter-weight route to ap-

proximate designs; determining the minimal perturbation strength and its scaling with system size remains open. (iii) Symmetries and sectors: With conservation laws or fixed-sector dynamics [47, 48], how do symmetry constraints modify the attainable design order and the required switch time  $t_s$ ? What changes if the post-quench ensemble or the charge sector differs from the pre-quench one? (iv) Transition-like behavior: Varying the ratio of random to deterministic couplings could induce sharp crossovers—or bona fide transitions—in "designability," potentially correlated with underlying dynamical or spectral transitions. (v) Experimental integration: The protocol is naturally compatible with randomized measurements (OTOCs, entanglement probes), since the Hamiltonian already realized on hardware can generate near-Haar unitaries after a single parameter switch. Identifying optimal operating points—balancing total evolution time, error tolerance, and control noise—would directly benefit current platforms. (vi) Beyond Hamiltonian: The single-quench principle suggests circuitlevel analogs—one-shot reconfigurations of gate ensembles—that approach Haar moments with minimal spatiotemporal modulation, offering an alternative to fully Brownian schemes. An important question is how the requirement  $t_s \gtrsim t_{\rm Th}$  translates into an equivalent depth or light-cone condition in random-circuit implementations. (vii) Lindbladian evolution: Does the single-quench idea extend to open, Markovian dynamics? Can one quench dissipative rates or the Lindbladian generator to realize approximate unitary k-designs—or channel k-designs over CPTP maps? (viii) Strong designs: Can singlequench evolution realize strong unitary designs [87–89], and under what spectral or mixing conditions?

Overall, the single-quench approach provides a minimal-control pathway to high-quality pseudorandomness. Mapping its performance across symmetry classes, degrees of integrability breaking, and architectures—and establishing rigorous finite-size and finite-time error bounds for approximate k-designs—are natural next steps with clear theoretical and experimental payoff.

Acknowledgments—We thank Thierry Giamarchi, Romain Vasseur, Laura Foini, Chang Liu, Tian-Gang Zhou, Pengfei Zhang, and Liang Mao for helpful discussions. This work has received support through the Swiss Quantum Initiative awarded by the State Secretariat for Economic Affairs, under the grant "Holo-Graph". This research is supported in part by the Fonds National Suisse de la Recherche Scientifique (Schweizerischer Nationalfonds zur Förderung der wissenschaftlichen Forschung) through the Project Grant 200021\_215300 and the NCCR51NF40-141869 The Mathematics of Physics (SwissMAP).

## Appendix A: Computation of the error of FP from single-quench to multiple-quench

In this appendix, we provide a detailed computation of the FP of the quench multiple times evolution protocol. In realistic settings where the Hilbert space dimension is finite, one needs to reach a unitary k-design up to a small error  $\epsilon$ . We say an ensemble  $\varepsilon$  on U(d) is an  $\delta$ -approximate unitary k-design if its k-FP obeys

$$F_{\varepsilon}^{(k)} - F_{\mathrm{Haar}}^{(k)} \leq \delta.$$

For an ensemble  $\varepsilon \subset U(d)$ , define its (k,k) moment operator

$$\Phi \equiv \Phi_{\varepsilon}^{(k)} = \mathbb{E}_{U \sim \varepsilon} [U^{\otimes k} \otimes U^{* \otimes k}],$$

which is Hermitian, positive semidefinite, with  $\|\Phi\|_{op} \leq 1$ . Let  $\Pi$  denote the Haar moment operator;  $\Pi$  is a projector with

$$\Pi^2 = \Pi, \qquad \operatorname{Tr} \Pi = \operatorname{Tr} \Pi^2 = F_{\operatorname{Haar}}^{(k)} = \begin{cases} k!, & d \ge k, \\ \sum_{\lambda \vdash k, \ \ell(\lambda) \le d} (f^{\lambda})^2, & d < k. \end{cases}$$

The k-th FP is

$$F_{\varepsilon}^{(k)} = \mathbb{E}_{U,V \sim \varepsilon} |\operatorname{Tr}(U^{\dagger}V)|^{2k} = \operatorname{Tr}(\Phi^2).$$

Assume the single-quench protocol produces an ensemble  $\varepsilon$  with

$$F_{\varepsilon}^{(k)} = F_{\mathrm{Haar}}^{(k)} + \delta \quad \Longleftrightarrow \quad \mathrm{Tr} \big[ (\Phi - \Pi + \Pi)^2 \big] = F_{\mathrm{Haar}}^{(k)} + \delta.$$

Work in a basis splitting the Haar subspace and its orthogonal complement:

$$\Phi = \Pi \oplus \operatorname{diag}(\mu_1, \mu_2, \ldots), \quad 0 \leq \mu_i \leq 1.$$

Then

$$F_{\varepsilon}^{(k)} = F_{\mathrm{Haar}}^{(k)} + \sum_{i} \mu_{i}^{2} \quad \Rightarrow \quad \sum_{i} \mu_{i}^{2} = \delta.$$

For the quench-3-time statistic, set  $A = U_1U_2$ ,  $B = U_3U_4$  with i.i.d. draws  $U_j \sim \varepsilon$ . Then A, B are independent with distribution  $\varepsilon^{*2}$  (convolution), hence

$$\mathbb{E}_{U_1,\dots,U_4\sim\varepsilon} \left| \text{Tr}(U_1 U_2 U_3^{\dagger} U_4^{\dagger}) \right|^{2k} = F_{\varepsilon^{*2}}^{(k)}.$$

Under convolution, moment operators multiply:

$$\Phi(\varepsilon^{*2}) = \Phi(\varepsilon)^2 = \Phi^2,$$

so

$$F_{\varepsilon^{*2}}^{(k)}=\mathrm{Tr}\!\big(\Phi(\varepsilon^{*2})^2\big)=\mathrm{Tr}(\Phi^4).$$

In the same eigenbasis,

$$\Phi^4 = \Pi \oplus \text{diag}(\mu_1^4, \mu_2^4, \ldots),$$

and we obtain the exact identity

$$\mathbb{E} \left| \text{Tr}(U_1 U_2 U_3^{\dagger} U_4^{\dagger}) \right|^{2k} = F_{\text{Haar}}^{(k)} + \sum_i \mu_i^4$$
 (19)

with  $\sum_i \mu_i^2 = \delta$ . Because  $0 \le \mu_i^4 \le \mu_i^2$  and by Cauchy-Schwarz  $\sum_i \mu_i^4 \le (\sum_i \mu_i^2)^2 = \delta^2$ ,

$$F_{\text{Haar}}^{(k)} \le F_{\varepsilon^{*2}}^{(k)} \le F_{\text{Haar}}^{(k)} + \min\{\delta, \delta^2\}.$$
 (20)

Thus, the FP excess above Haar cannot increase under one convolution step, and when  $\delta \ll 1$  it improves quadratically: the four-draw statistic is closer to  $F_{\rm Haar}^{(k)}$  than the two-draw one.

Consider then using iterating quenches to reach an approximate k-design. After  $M=2^m-1$  independent quenches

Consider then using iterating quenches to reach an approximate k-design. After  $M = 2^m - 1$  independent quenches (i.e.,  $2^m$  draws and  $2^{m-1}$  convolutions),

$$\Phi \longmapsto \Phi^{2^{m-1}}, \qquad F_k(\varepsilon^{*2^{m-1}}) = \text{Tr}(\Phi^{2^{m-1}}) = F_{\text{Haar}}^{(k)} + \sum_i \mu_i^{2^{m-1}}.$$

Hence for small  $\delta$ ,

$$0 \le F_k(\varepsilon^{*(2^{m-1})}) - F_{\text{Haar}}^{(k)} \le \left(\sum_i \mu_i^2\right)^{2^{m-1}} = \delta^{2^{m-1}}.$$

To achieve an  $\epsilon$ -approximate k-design it suffices that  $\delta^{2^{m-1}} \leq \epsilon$ , i.e.

$$M \ge 2 \frac{\log(1/\epsilon)}{\log(1/\delta)} - 1. \tag{21}$$

Thus, the number of quenches grows only logarithmically with the target accuracy (for fixed initial gap  $\delta$ ), a favorable scaling for experiments.

#### Appendix B: Computation of the frame potential of single-quench GUE evolution

This appendix provides a step-by-step derivation of the first-order frame potential for a single-quench evolution generated by Gaussian Unitary Ensemble (GUE) Hamiltonians.

Definition. For a single uninterrupted (no quench) evolution, the first-order frame potential is

$$F^{(1)}(t) = \int dH_1 dH_2 P(H_1) P(H_2) \left| \text{Tr} \left( e^{iH_1 t} e^{-iH_2 t} \right) \right|^2.$$
 (22)

For a single quench at time  $t_s \in [0, t]$ , we write the two segments explicitly and duplicate the Hamiltonians for the complex conjugate trace:

$$F^{(1)}(t;t_s) = \int \left( \prod_{a=1}^4 dH_a P(H_a) \right) \left| \text{Tr} \left( e^{iH_1(t-t_s)} e^{iH_2t_s} e^{-iH_3t_s} e^{-iH_4(t-t_s)} \right) \right|^2.$$
 (23)

Here  $P(H_j) = e^{-\frac{d}{2}\text{Tr}(H_j^2)}$  is the GUE measure and d denotes the Hilbert-space dimension.

Diagonalization and unitary invariance. Use the spectral decompositions

$$e^{iH_a\tau_a} = V_a\Lambda^{(a)}V_a^{\dagger}, \qquad \Lambda^{(a)} = \operatorname{diag}(e^{i\lambda_1^{(a)}\tau_a}, \dots, e^{i\lambda_d^{(a)}\tau_a}), \tag{24}$$

with segment durations  $(\tau_1, \tau_2, \tau_3, \tau_4) = (t - t_s, t_s, -t_s, -(t - t_s))$ . By unitary-conjugation invariance of GUE, the joint distribution factorizes into eigenvalues and independent Haar unitaries for the eigenvectors. Defining

$$U^{1} = V_{1}^{\dagger} V_{2}, \quad U^{2} = V_{2}^{\dagger} V_{3}, \quad U^{3} = V_{3}^{\dagger} V_{4}, \quad U^{4} = (U^{1} U^{2} U^{3})^{\dagger},$$
 (25)

and denoting  $D\lambda_a$  the induced eigenvalue measures, the trace becomes

$$F^{(1)}(t;t_s) = \int \left( \prod_{a=1}^4 D\lambda_a \right) \int_{\text{Haar}} dU^1 dU^2 dU^3 \operatorname{Tr} \left( \Lambda^{(1)\dagger} U^1 \Lambda^{(2)\dagger} U^2 \Lambda^{(3)} U^3 \Lambda^{(4)} U^4 \right)$$

$$\times \operatorname{Tr} \left( U^{4\dagger} \Lambda^{(4)\dagger} U^{3\dagger} \Lambda^{(3)\dagger} U^{2\dagger} \Lambda^{(2)} U^{1\dagger} \Lambda^{(1)} \right).$$
(26)

Index expansion and Haar integration. Writing the two traces with explicit indices, e.g.

$$\operatorname{Tr}(\Lambda^{(1)\dagger}U^{1}\Lambda^{(2)\dagger}U^{2}\Lambda^{(3)}U^{3}\Lambda^{(4)}U^{4}) = \Lambda^{(1)*}_{i_{1}}U^{1}_{i_{1}i_{2}}\Lambda^{(2)*}_{i_{2}}U^{2}_{i_{2}i_{3}}\Lambda^{(3)}_{i_{3}}U^{3}_{i_{3}i_{4}}\Lambda^{(4)}_{i_{4}}U^{4}_{i_{4}i_{1}}, \tag{27}$$

and similarly for the conjugate trace, the averages over  $U^1, U^2, U^3$  factorize and can be performed with the second-moment Weingarten formula,

$$\int_{\text{Haar}} dU \ U_{i\alpha} U_{j\beta}^* U_{k\gamma} U_{l\delta}^* = \frac{\delta_{ij} \delta_{\alpha\beta} \delta_{kl} \delta_{\gamma\delta} + \delta_{il} \delta_{\alpha\delta} \delta_{kj} \delta_{\gamma\beta}}{d^2 - 1} - \frac{\delta_{ij} \delta_{\alpha\delta} \delta_{kl} \delta_{\gamma\beta} + \delta_{il} \delta_{\alpha\beta} \delta_{kj} \delta_{\gamma\delta}}{d(d^2 - 1)}.$$
 (28)

Applying Eq. (28) independently to  $U^1$ ,  $U^2$ , and  $U^3$ , one organizes the resulting contractions into a 1/d expansion. The leading terms are either (i) fully "disconnected" (no phase correlations between segments), or (ii) products of "connected" pairings that are precisely the spectral form factors of the individual segments.

Eigenvalue integrals and leading behavior. Introduce the (two-point) spectral form factor (SFF)

$$R_2(\tau) = \left\langle \left| \text{Tr}(e^{iH\tau}) \right|^2 \right\rangle_{H \sim \text{GUE}} = \left\langle \sum_{a,b=1}^d e^{i(\lambda_a - \lambda_b)\tau} \right\rangle, \tag{29}$$

so that the leading large-d contribution to Eq. (26) reads

$$F^{(1)}(t;t_s) = \frac{d^6}{(d^2 - 1)^3} + \frac{d^8}{(d^2 - 1)^3} \left(\frac{R_2(t - t_s)}{d^2}\right)^2 \left(\frac{R_2(t_s)}{d^2}\right)^2 + \mathcal{O}(\frac{1}{d}) = 1 + d^2 \left(\frac{R_2(t - t_s)}{d^2}\right)^2 \left(\frac{R_2(t_s)}{d^2}\right)^2 + \mathcal{O}(\frac{1}{d}).$$
(30)

Setting  $t_s = t$  recovers the single-segment (no-quench) result. The eigenvalue measures  $D\lambda_a$  are those induced by GUE; only the SFFs survive at leading order.

GUE spectral form factor. For GUE (with the standard Wigner semicircle scaling), one may write

$$R_2(t) = d + d^2 r_1(t)^2 + d r_2(t), \qquad r_1(t) = \frac{J_1(2t)}{t},$$
 (31)

where  $r_1(t) \sim t^{-3/2}$  for  $t \gg 1$  and  $r_2(t)$  encodes the connected "ramp" contribution. Equivalently,

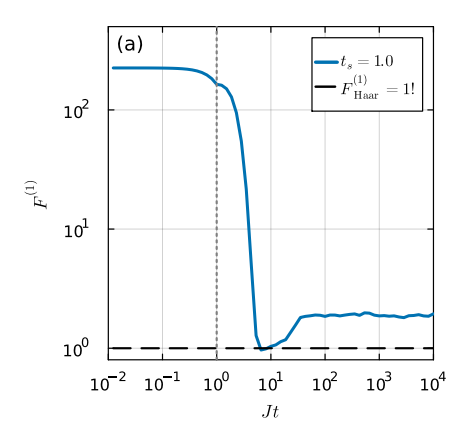
$$\frac{R_2(t)}{d^2} = r_1(t)^2 + \mathcal{O}(\frac{t}{d^2}). \tag{32}$$

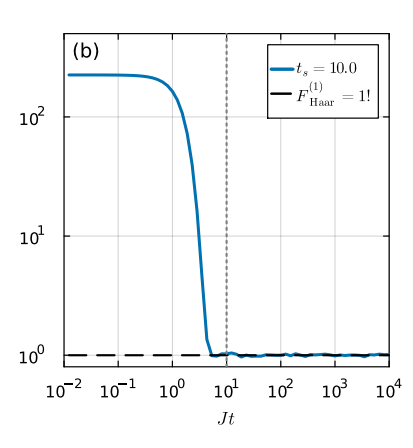
The qualitative time dependence is

$$R_2(t) \sim \begin{cases} d^2, & t \ll t_{\rm Th}, \\ \sqrt{d}, & t \sim t_{\rm Th}, \\ d, & t \gtrsim t_p, \end{cases}$$

$$(33)$$

where  $t_{\rm Th}$  is the Thouless time and  $t_p$  the plateau time.





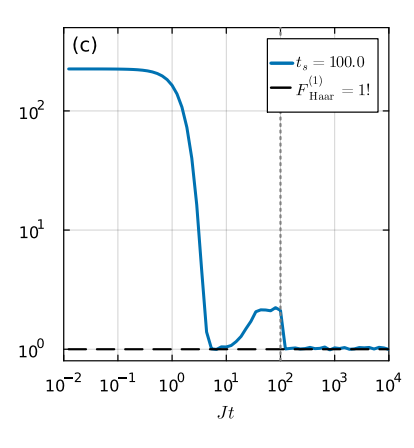


FIG. 5. First-order frame potential  $F^{(1)}$  versus total evolution time for single-quench dynamics of the complex-fermion SYK<sub>2</sub> model in a fixed charge sector. Parameters: N=6, q=2, J=1; averages over  $10^4$  disorder realizations. The Haar-random benchmark  $F^{(1)}=1$  is shown as a black dashed curve. The switch time  $t_s$  is indicated by a gray dot vertical line in each panel: (a)  $Jt_s=1.0$  (before the Thouless time  $t_{\rm Th}$ ), (b)  $Jt_s=10.0$  (near  $t_{\rm Th}$ ), and (c)  $Jt_s=100.0$  (after  $t_{\rm Th}$ ). At late times, the plateau of  $F^{(2)}$  lies above the Haar value for  $t_s < t_{\rm Th}$ , while it saturates the Haar value when  $t_s \approx t_{\rm Th}$  or  $t_s > t_{\rm Th}$ .

Consequence for the frame potential. Inserting Eq. (31) into Eq. (30) shows that, when the switch time satisfies  $t_s \gtrsim t_{\rm Th}$ , both  $R_2(t_s)/d^2$  and  $R_2(t-t_s)/d^2$  are bounded by  $\mathcal{O}(1/d)$  as  $d \to \infty$ , hence the second term in Eq. (30) vanishes in the thermodynamic limit. Consequently, the frame potential attains the Haar value,

$$\lim_{d \to \infty} F^{(1)}(t; t_s) = 1, \tag{34}$$

i.e., the single-quench GUE evolution realizes a unitary 1-design.

#### Appendix C: The single-quench evolution of integrable models

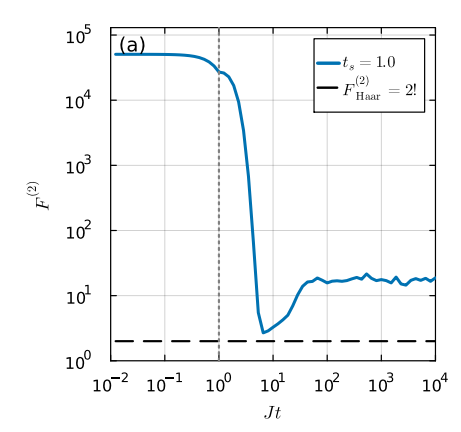
This appendix presents additional numerics for the frame potential (FP) under the single-quench evolution in *integrable* models. We consider (i) the SYK<sub>2</sub> model, which is free and integrable, and (ii) the Richardson model, which is interacting yet integrable.

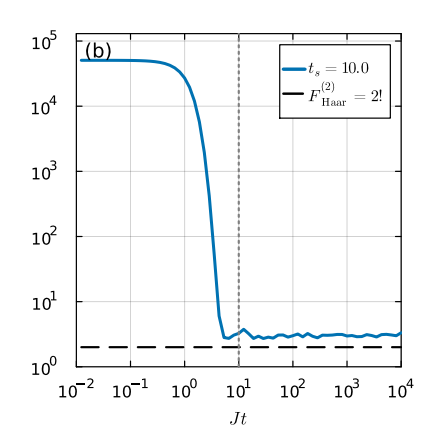
SYK<sub>2</sub> model (free, integrable).

The Hamiltonian of the complex SYK<sub>2</sub> model is

$$H = i \sum_{1 \le j < k \le N} J_{jk} c_j^{\dagger} c_k \tag{35}$$

with  $J_{ij}$  a random tensor of rank two whose probability distribution is Gaussian with zero mean. Let  $t_s$  denote the switch time and  $t_{\rm Th}$  the Thouless time. For  $t_s \geq t_{\rm Th}$ , the first-order frame potential  $F^{(1)}$  saturates the Haar value at late times, whereas higher-order frame potentials  $F^{(k>1)}$  do not. As shown in Fig. 5, when  $t_s \gtrsim t_{\rm Th}$  the curve for  $F^{(1)}$  reaches the Haar plateau [Fig. 5(b) and (c)], indicating realization of a unitary 1-design; for  $t_s < t_{\rm Th}$  the late-time plateau lies above the Haar value [Fig. 5 (a)], so a 1-design is not achieved. Moreover, Fig. 6 shows that  $F^{(2)}$  in the complex SYK<sub>2</sub> model fails to reach its Haar value for any  $t_s$  (before or after  $t_{\rm Th}$ ). Instead, it saturates at the so-called Gaussian Haar value [48], which indicates that the single-quench model can still realize Brownian dynamics after the quench. More information on this can be found in SM [80]. Thus, under the single-quench protocol, the integrable SYK<sub>2</sub> ensemble realizes a unitary 1-design but no higher designs, in contrast to the chaotic SYK<sub>4</sub> case. This supports the achievable design order as an operational diagnostic of chaos.





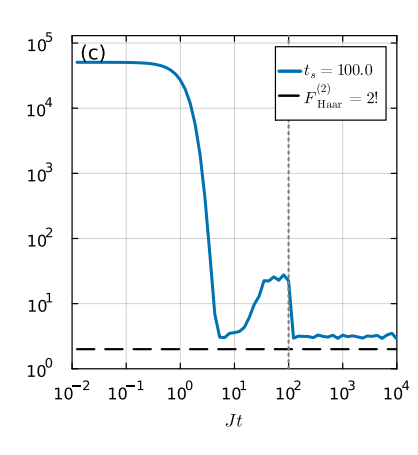


FIG. 6. First-order frame potential  $F^{(2)}$  versus total evolution time for single-quench dynamics of the complex-fermion SYK<sub>2</sub> model in a fixed charge sector. Parameters: N=6, q=2, J=1; averages over  $10^4$  disorder realizations. The Haar-random benchmark  $F^{(2)}=2$  is shown as a black dashed curve. The switch time  $t_s$  is indicated by a gray dot vertical line in each panel: (a)  $Jt_s=1.0$  (before the Thouless time  $t_{\rm Th}$ ), (b)  $Jt_s=10.0$  (near  $t_{\rm Th}$ ), and (c)  $Jt_s=100.0$  (after  $t_{\rm Th}$ ). At late times, the plateau of  $F^{(2)}$  lies above the Haar value for all different  $t_s$ .

## Richardson model (interacting, integrable).

For the Richardson model with random single-particle energies  $\{\epsilon_i\}$ , the Hamiltonian is

$$H = \frac{J}{N} \sum_{i,j=1}^{N} S_i^+ S_j^- + \sum_{j=1}^{N} \epsilon_j S_j^z.$$
 (36)

There exists a complete set of mutually commuting Gaudin charges  $R_i(\epsilon)$  such that  $[R_i, R_j] = 0$  and  $[H, R_i] = 0$ ; in fact, H lies in the linear span of  $R_i$ . The model is therefore integrable—interacting, yet endowed with randomness through  $\epsilon_j$ . Here, the prefactor 1/N ensures that both terms in the Hamiltonian scale equally in the large-N limit.

The first order FP of the Richardson model as a function of total evolution time is illustrated in Fig. 7, and it shows that its  $F^{(1)}$  fails to reach its Haar value for any  $t_s$  (before or after  $t_{\rm Th}$ ). Thus, under the single-quench protocol, this random integrable and interacting model fails to realize even a unitary 1-design. Compared with the complex SYK<sub>2</sub> model, which is integrable and free but able to realize a 1-design, this integrable but interacting model fails to realize a 1-design, which is interesting, and it could indicate that the SYK<sub>2</sub> model is more "random" than the Richardson model, although it is non-interacting.

Across these integrable examples, the single-quench evolution fails to realize higher ( $k \geq 2$ ) unitary designs even when the switch time exceeds the Thouless time. This supports the view that the ability of the protocol to produce a unitary design is a diagnostic of *chaos*: chaotic dynamics exhibit FP saturation at  $t_s \gtrsim t_{\rm Th}$ , whereas integrable dynamics do not.

## Appendix D: More numerical results about single-quench evolution of chaotic models

In this appendix, we present additional numerical results for single-quench dynamics in chaotic models, including the complex SYK<sub>4</sub> model, the complex SYK<sub>4</sub> model with reduced-rank couplings, and the Majorana SYK<sub>4</sub> model.

# Complex SYK<sub>4</sub> model

The first-, third-, and fourth-order FPs of the complex SYK<sub>4</sub> model are shown in Figs. 8, 9, and 10, respectively. As evident there, the single-quench evolution attains the Haar value once the switch time satisfies  $t_s \ge t_{\rm Th}$ , indicating that this protocol realizes (at least) a unitary 4-design.

Define the k-th order FP gap as

$$\Delta_{\text{FP}}^{(k)}(t_s) \equiv F^{(k)}(t_s \to \infty) - F_{\text{Haar}}^{(k)}, \qquad F_{\text{Haar}}^{(k)} = k!$$
 (37)

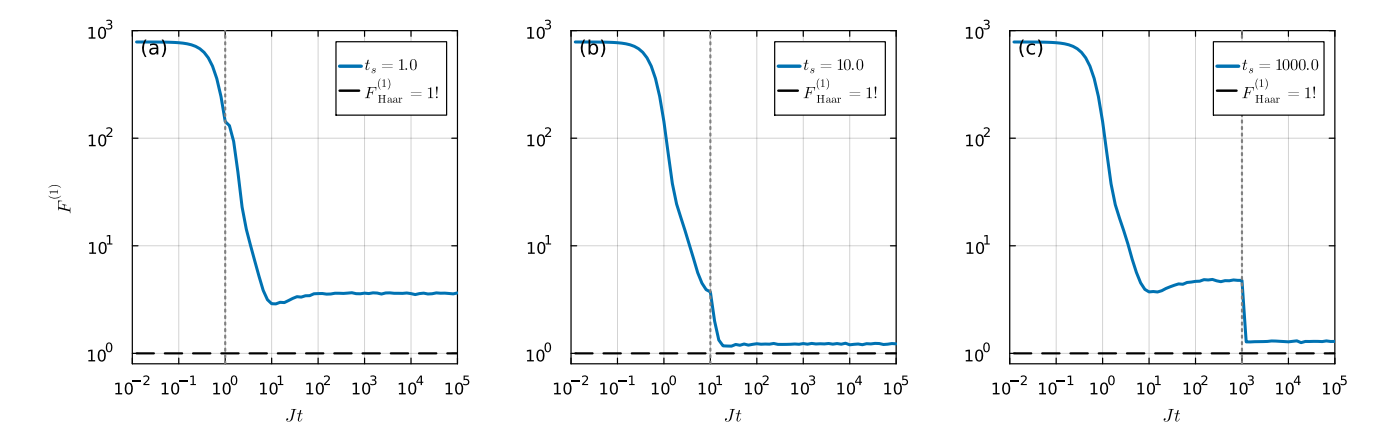


FIG. 7. First-order frame potential  $F^{(1)}$  versus total evolution time for single-quench dynamics of the Richardson model. Parameters: N=8, q=2, J=1; averages over  $10^4$  disorder realizations. The random local energy  $\{\epsilon_j\}$  is chosen to be Gaussian random with zero mean and variance  $\sigma=1$ . The Haar-random benchmark  $F^{(1)}=1$  is shown as a black dashed curve. The switch time  $t_s$  is indicated by a gray dashed vertical line in each panel: (a)  $t_s=1.0$  (before the Thouless time  $t_{\rm Th}$ ), (b)  $t_s=10.0$  (near  $t_{\rm Th}$ ), and (c)  $t_s=1000.0$  (after  $t_{\rm Th}$ ).

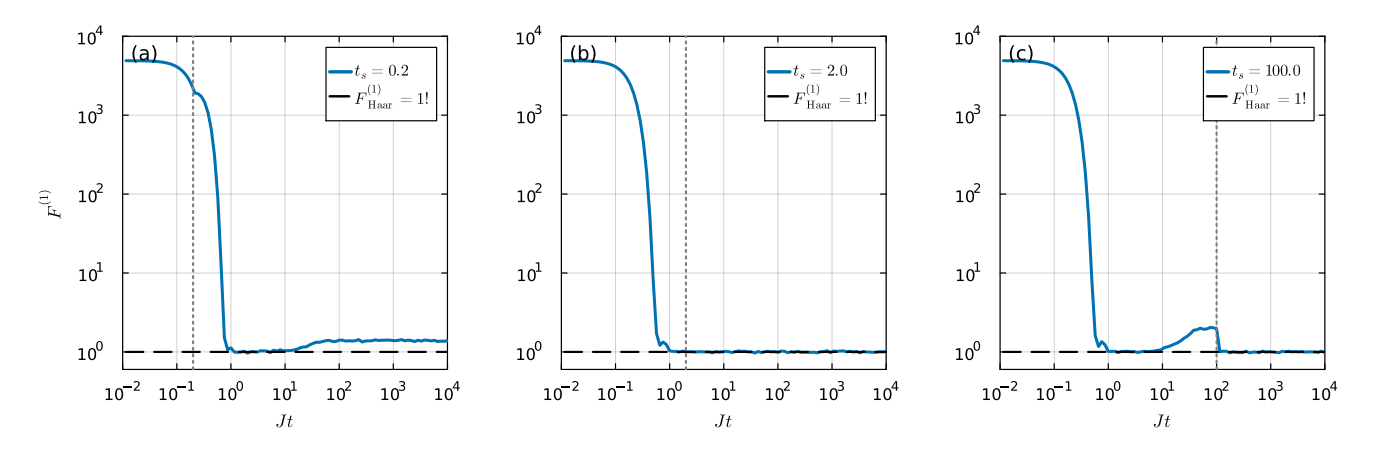


FIG. 8. First-order frame potential  $F^{(1)}$  versus total evolution time for single-quench dynamics of the complex-fermion SYK<sub>4</sub> model in a fixed charge sector. Parameters: N=8, q=4, J=1; averages over 4000 disorder realizations. The Haar-random benchmark  $F^{(1)}=1$  is shown as a black dashed curve. The switch time  $t_s$  is indicated by a gray dashed vertical line in each panel: (a)  $t_s=0.2$  (before the Thouless time  $t_{\rm Th}$ ), (b)  $t_s=2.0$  (near  $t_{\rm Th}$ ), and (c)  $t_s=100.0$  (after  $t_{\rm Th}$ ). At late times, the plateau of  $F^{(1)}$  lies above the Haar value for  $t_s< t_{\rm Th}$ , while it saturates the Haar value when  $t_s\approx t_{\rm Th}$  or  $t_s>t_{\rm Th}$ .

Figs. 11 and 12 display  $\Delta_{\text{FP}}^{(2)}(t_s)$  and  $\Delta_{\text{FP}}^{(3)}(t_s)$  versus the switch time  $t_s$  for the single-quench evolution of the complex SYK<sub>4</sub> model. The gap decreases to zero at the Thouless time, furnishing an operational definition of  $t_{\text{Th}}$ . In agreement with the first-order FP figure Fig. 3 in the main text, the resulting  $t_{\text{Th}}$  is independent of the FP order k.

#### Complex SYK<sub>4</sub> model with reduced-rank couplings

We also consider the SYK model with reduced rank coupling whose Hamiltonian is given by [90]

$$H = \sum_{1 \le i \le k \le l \le N} J_{ijkl}^{red} c_i^{\dagger} c_j^{\dagger} c_k c_l, \tag{38}$$

and  $J_{ijkl}^{red} = J_{ik}J_{jl} - J_{il}J_{jk}$  with  $J_{ij}$  a random tensor of rank two whose probability distribution is (approximately) Gaussian. This model is more friendly to experimental realization of the SYK model [91]. Its single-quench time evolution can also satisfy unitary 2-designs, as shown in Fig. 13.

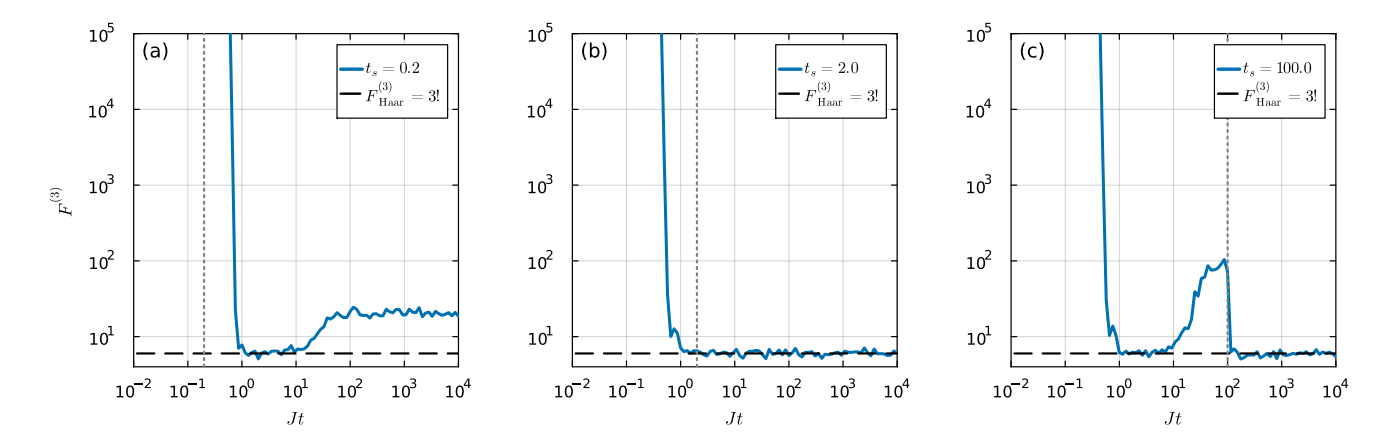


FIG. 9. Third-order frame potential  $F^{(3)}$  versus total evolution time for single-quench dynamics of the complex-fermion SYK<sub>4</sub> model in a fixed charge sector. Parameters: N=8, q=4, J=1; averages over 4000 disorder realizations. The Haar-random benchmark  $F^{(3)}=3!$  is shown as a black dashed curve. The switch time  $t_s$  is indicated by a gray dot vertical line in each panel: (a)  $Jt_s=0.2$  (before the Thouless time  $t_{\rm Th}$ ), (b)  $Jt_s=2.0$  (near  $t_{\rm Th}$ ), and (c)  $Jt_s=100.0$  (after  $t_{\rm Th}$ ).

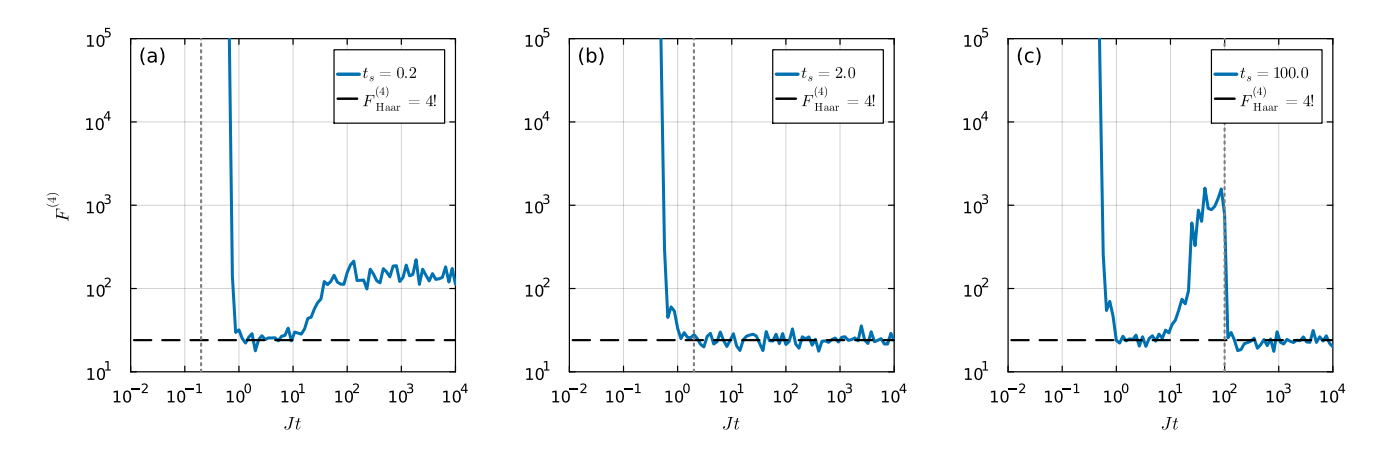


FIG. 10. Fourth-order frame potential  $F^{(4)}$  versus total evolution time for single-quench dynamics of the complex-fermion SYK<sub>4</sub> model in a fixed charge sector. Parameters: N=8, q=4, J=1; averages over 4000 disorder realizations. The Haar-random benchmark  $F^{(4)}=4!$  is shown as a black dashed curve. The switch time  $t_s$  is indicated by a gray dot vertical line in each panel: (a)  $Jt_s=0.2$  (before the Thouless time  $t_{\rm Th}$ ), (b)  $Jt_s=2.0$  (near  $t_{\rm Th}$ ), and (c)  $Jt_s=100.0$  (after  $t_{\rm Th}$ ).

# ${\bf Majorana~SYK_4~model}$

The Hamiltonian of the Majorana  $SYK_4$  model is

$$H = \sum_{i,j,k,l=1}^{N} J_{ijkl} \chi_i \chi_j \chi_k \chi_l$$

with Majorana fermions  $\{\chi_i, \chi_j\} = 2\delta_{ij}$ . Its single-quench time evolution saturates the plateau value  $2^k k!$ , as shown in Fig. 14. The additional factor  $2^k$  relative to the Haar value arises from the Majorana symmetry factor.

#### Appendix E: Single-Quench vs. Brownian SYK

In this section, we give a short overview of some analytic results for complex Brownian SYK that have previously been studied in [47, 48]. They can be used to benchmark the long-time behavior of the single-quench evolution, as our numerical data imply agreement with the Brownian case. For complex SYK<sub>4</sub>, this agreement is expected, as both the Brownian evolution and our single-quench model saturate the Haar value k!. For SYK<sub>2</sub>, however, this is a stronger

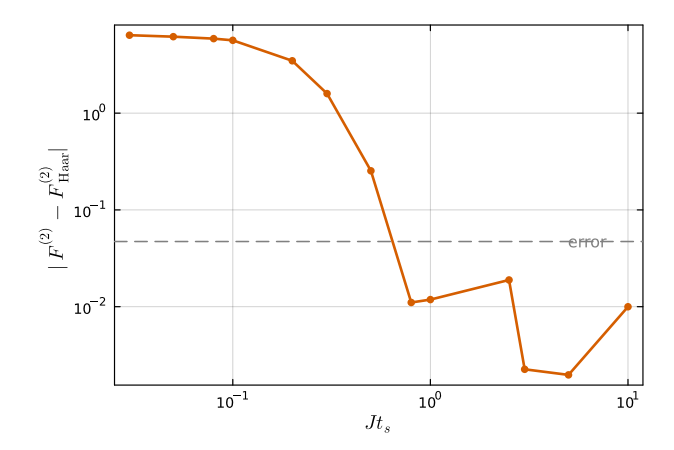


FIG. 11. Gap  $\Delta_{\mathrm{FP}}(t_s)$  between the late-time plateau of the first-order frame potential  $F^{(2)}$  and its Haar value for single-quench evolution of the complex SYK<sub>4</sub> model in a fixed charge sector, plotted versus the switch time  $t_s$ . Parameters: N=6, total charge q=2, J=1; averaged over  $N_{\mathrm{rand}}=10^4$  disorder realizations. The Thouless time  $t_{\mathrm{Th}}$  is defined as the first  $t_s$  at which  $\Delta_{\mathrm{FP}}(t_s)$  is consistent with zero within the statistical uncertainty (gray dashed line). The uncertainty is estimated as  $\sqrt{(4!-2!)/[\sqrt{N_{\mathrm{rand}}}(\sqrt{N_{\mathrm{rand}}}-1)]} \simeq 0.047$ .

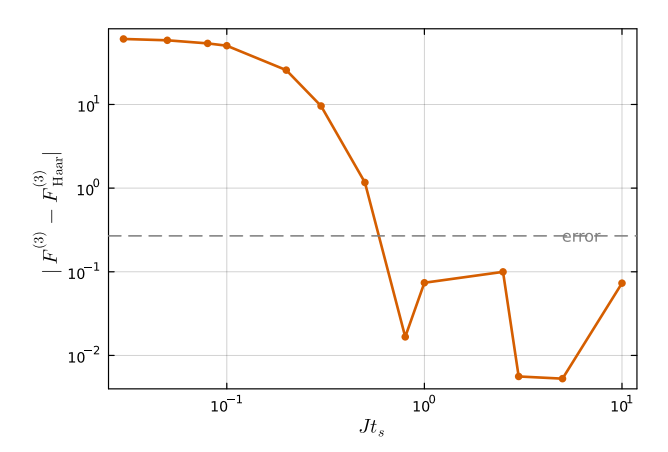


FIG. 12. Gap  $\Delta_{\mathrm{FP}}(t_s)$  between the late-time plateau of the first-order frame potential  $F^{(3)}$  and its Haar value for single-quench evolution of the complex SYK<sub>4</sub> model in a fixed charge sector, plotted versus the switch time  $t_s$ . Parameters: N=6, total charge  $q=2,\ J=1$ ; averaged over  $N_{\mathrm{rand}}=10^4$  disorder realizations. The Thouless time  $t_{\mathrm{Th}}$  is defined as the first  $t_s$  at which  $\Delta_{\mathrm{FP}}(t_s)$  is consistent with zero within the statistical uncertainty (gray dashed line). The uncertainty is estimated as  $\sqrt{(6!-3!)/[\sqrt{N_{\mathrm{rand}}}(\sqrt{N_{\mathrm{rand}}}-1)]}\simeq 0.27$ .

result. Whether a single quench reproduces the Brownian average in general — e.g., for a larger class of integrable models that do not scramble to the Haar value — is a question we postpone for future work. For the Brownian model, we can consider again the Hamiltonians 6 and 35 but with time dependent couplings  $J_{ijkl}(t)$ 

For the Brownian model, we can consider again the Hamiltonians 6 and 35 but with time dependent couplings  $J_{ijkl}(i)$  and  $J_{ij}(t)$  s.t.

$$\langle J_{ijkl}(t)J_{i'j'k'l'}(t')\rangle = \delta_{i,i'}\delta_{j,j'}\delta_{k,k'}\delta_{l,l'}\delta(t-t')\frac{3!J^2}{N^3} \quad \text{and} \quad \langle J_{ij}(t)J_{i'j'}(t')\rangle = \delta_{i,i'}\delta_{j,j'}\delta(t-t')\frac{J^2}{N}.$$

This model allows a convenient calculation of the Frame potential in terms of a path integral. We just need to notice that the forward-backward evolution  $U^{\dagger}(t)V(t)$  can be effectively written as forward-only evolution U(2t) because the couplings are gaussian variables centered around zero, rendering the sign irrelevant.

The calculation proceeds by summing the contributions from the classical saddle-points of the path integral. For SYK<sub>4</sub>, this task is straightforward (see [47] for Majorana SYK and [48] for the complex case). For the late time

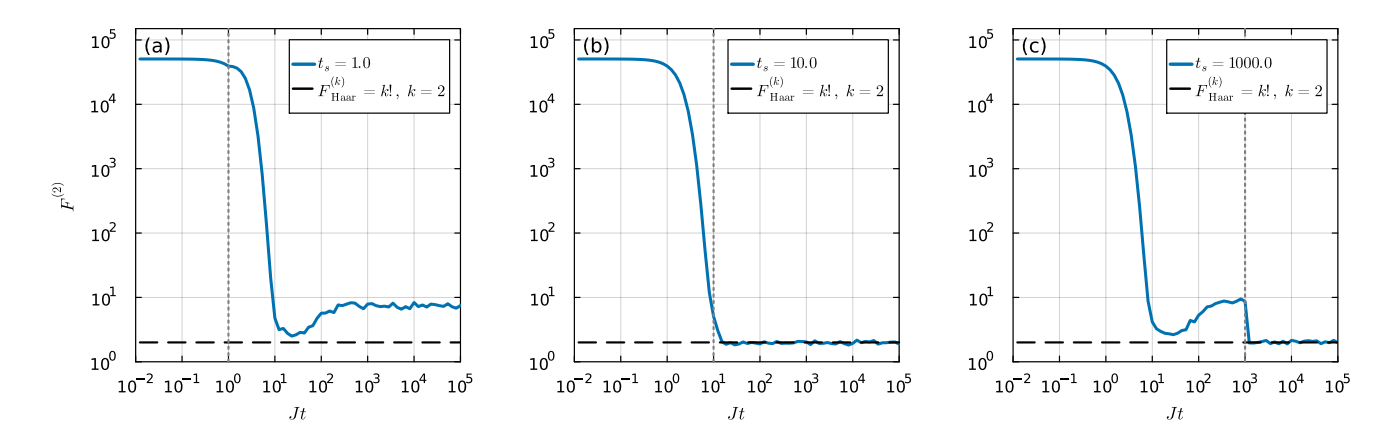


FIG. 13. Second-order frame potential  $F^{(2)}$  versus total evolution time for single-quench dynamics of the complex-fermion SYK<sub>4</sub> model with reduced rank couplings in a fixed charge sector. Parameters: N = 6, q = 2, J = 1; averages over  $10^4$  disorder realizations. The Haar-random benchmark  $F^{(2)} = 2$  is shown as a black dashed curve. The switch time  $t_s$  is indicated by a gray dashed vertical line in each panel: (a)  $t_s = 1.0$  (before the Thouless time  $t_{\rm Th}$ ), (b)  $t_s = 10.0$  (near  $t_{\rm Th}$ ), and (c)  $t_s = 1000.0$  (after  $t_{\rm Th}$ ). At late times, the plateau of  $F^{(2)}$  lies above the Haar value for  $t_s < t_{\rm Th}$ , while it saturates the Haar value when  $t_s \approx t_{\rm Th}$  or  $t_s > t_{\rm Th}$ .

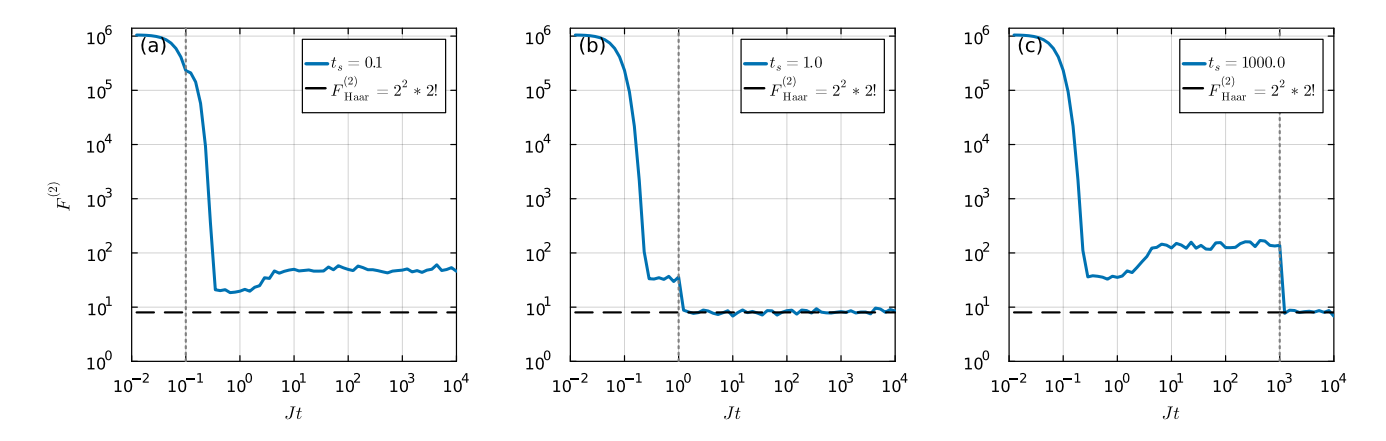


FIG. 14. Second-order frame potential  $F^{(2)}$  versus total evolution time for single-quench dynamics of the Majorana SYK<sub>4</sub> model. Parameters: N=5, J=1; averages over  $10^3$  disorder realizations. The Haar-random benchmark  $F^{(k)}=2^kk!$  for k=2 is shown as a black dashed curve. The switch time  $t_s$  is indicated by a gray dashed vertical line in each panel: (a)  $t_s=0.1$  (before the Thouless time  $t_{\rm Th}$ ), (b)  $t_s=1.0$  (near  $t_{\rm Th}$ ), and (c)  $t_s=1000.0$  (after  $t_{\rm Th}$ ). At late times, the plateau of  $F^{(2)}$  lies above the Haar value for  $t_s < t_{\rm Th}$ , while it saturates the Haar value (up to the symmetry factor  $2^k$ ) when  $t_s \approx t_{\rm Th}$  or  $t_s > t_{\rm Th}$ .

evolution they indeed find [92]

$$F_{\mathrm{cSYK}_4}^{(k)}(T \to \infty) = k!$$

which confirms that Brownian evolution saturates the Haar value. For SYK<sub>2</sub>, the situation is more complicated. The problem is that the effective action appearing in the path integral exhibits a continuous  $U(k) \times U(k)$  symmetry that is broken down to SU(k) by the solution, which leads to additional Goldstone modes that activate higher order modes in the saddle point evaluation. In [48] et al., was found that the long time behavior of the Frame potential scales as

$$F_{\mathrm{SYK}_2}^{(k)}(T \to \infty) \sim N \cdot N^{k^2 - 1}$$

where  $k^2 - 1$  is the number of massless Goldstone modes. Note that the Frame potential has been taken over all charged sectors here, which gives the additional factor of N.

For large-N, this approaches the Frame potential of so-called Gaussian Haar Unitaries. That means, instead of a general U, we take  $U = e^{iJ_{ij}c_i^{\dagger}c_j}$  where  $J_{ij}$  is a gaussian-valued hermitian matrix and we average over  $J_{ij}$ . The result

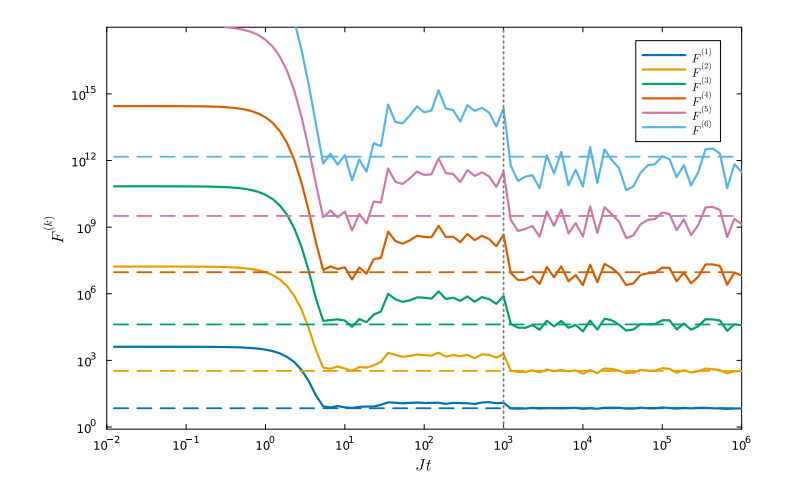


FIG. 15. Frame potential of complex SYK<sub>2</sub> for all charged sectors and for k = 1 to k = 6 with N = 6 fermions (3000 realizations). The colored dashed lines show the Gaussian Haar value (see eqn. 39). The grey dashed line indicates the switch time. Although the Gaussian Haar value becomes the Brownian SYK<sub>2</sub> value only for large N, it is still a good approximation at low N and for low k. It can be seen in the plots that it is also the drop-off value of the single-quench model after the quench. Only for k = 6, we can see a clear deviation, which is due to the low N regime we are working in. We can therefore conclude that the single-quench model effectively becomes the Brownian model.

reads [48]

$$F_{\text{Gauss}}^{k} = \prod_{n=0}^{N-1} \frac{\Gamma(n+2k+1)\Gamma(n+1)}{\Gamma(n+k+1)^{2}}.$$
 (39)

For large N, the relative Frame potential  $F^{(k)}(T)/F^{(k)}(0)$  with  $F^{(k)}(0)=2^{Nk}$  can be approximated by

$$\lim_{N \to \infty} \left(\frac{1}{N} \log \left(2^{-Nk} F_{\mathrm{Gauss}}^{(k)}\right)\right) \sim -k \log(2) + k^2 \frac{\log(N)}{N} \sim \lim_{N \to \infty} \left(\frac{1}{N} \log \left(2^{-Nk} F_{\mathrm{SYK}_2}^{(k)}(T \to \infty)\right)\right)$$

This approximation also holds well for small N and k, as shown in Fig. 15.

- \* zhouyn.physics@gmail.com † julian.sonner@unige.ch
- D. A. Roberts and B. Yoshida, Chaos and complexity by design, Journal of High Energy Physics 2017, 10.1007/jhep04(2017)121 (2017).
- [2] J. Cotler, N. Hunter-Jones, J. Liu, and B. Yoshida, Chaos, complexity, and random matrices, Journal of High Energy Physics 2017, 10.1007/jhep11(2017)048 (2017).
- [3] A. R. Brown and L. Susskind, Second law of quantum complexity, Physical Review D 97, 10.1103/physrevd.97.086015 (2018).
- [4] Z.-W. Liu, S. Lloyd, E. Zhu, and H. Zhu, Entanglement, quantum randomness, and complexity beyond scrambling, Journal of High Energy Physics 2018, 10.1007/jhep07(2018)041 (2018).
- [5] E. Bernstein and U. Vazirani, Quantum complexity theory, in Proceedings of the twenty-fifth annual ACM symposium on Theory of computing (1993) pp. 11–20.
- [6] H.-Y. Huang, R. Kueng, and J. Preskill, Predicting many properties of a quantum system from very few measurements, Nature Physics 16, 1050–1057 (2020).
- [7] A. Elben, R. Kueng, H.-Y. R. Huang, R. van Bijnen, C. Kokail, M. Dalmonte, P. Calabrese, B. Kraus, J. Preskill, P. Zoller, and B. Vermersch, Mixed-state entanglement from local randomized measurements, Phys. Rev. Lett. 125, 200501 (2020).
- [8] A. Elben, S. T. Flammia, H.-Y. Huang, R. Kueng, J. Preskill, B. Vermersch, and P. Zoller, The randomized measurement toolbox, Nature Reviews Physics 5, 9–24 (2022).
- [9] R. O'Donnell and J. Wright, Efficient quantum tomography, Proceedings of the forty-eighth annual ACM symposium on Theory of Computing (2015).
- [10] C. Portmann and R. Renner, Security in quantum cryptography, Reviews of Modern Physics 94, 025008 (2022), arXiv:2102.00021.
- [11] J. Emerson, R. Alicki, and K. Życzkowski, Scalable noise estimation with random unitary operators, Journal of Optics B: Quantum and Semiclassical Optics 7, S347–S352 (2005).
- [12] E. Knill, D. Leibfried, R. Reichle, J. Britton, R. B. Blakestad, J. D. Jost, C. Langer, R. Ozeri, S. Seidelin, and D. J. Wineland, Randomized benchmarking of quantum gates, Physical Review A 77, 10.1103/physreva.77.012307 (2008).
- [13] S. J. van Enk and C. W. J. Beenakker, Measuring  ${\rm Tr} \rho^n$  on single copies of  $\rho$  using random measurements, Phys. Rev. Lett. **108**, 110503 (2012).
- [14] B. Vermersch, A. Elben, L. Sieberer, N. Yao, and P. Zoller, Probing scrambling using statistical correlations between randomized measurements, Physical Review X 9, 10.1103/physrevx.9.021061 (2019).
- [15] A. Elben, B. Vermersch, C. F. Roos, and P. Zoller, Statistical correlations between locally randomized measurements: A toolbox for probing entanglement in many-body quantum states, Physical Review A 99, 10.1103/physreva.99.052323 (2019).
- [16] A. Elben, B. Vermersch, M. Dalmonte, J. I. Cirac, and P. Zoller, Rényi entropies from random quenches in atomic hubbard and spin models, Phys. Rev. Lett. 120, 050406 (2018).

- [17] M. K. Joshi, A. Elben, B. Vermersch, T. Brydges, C. Maier, P. Zoller, R. Blatt, and C. F. Roos, Quantum information scrambling in a trapped-ion quantum simulator with tunable range interactions, Physical Review Letters 124, 10.1103/physrevlett.124.240505 (2020).
- [18] F. Arute, K. Arya, R. Babbush, D. Bacon, J. C. Bardin, R. Barends, R. Biswas, S. Boixo, F. G. S. L. Brandao, D. A. Buell, B. Burkett, Y. Chen, Z. Chen, B. Chiaro, R. Collins, W. Courtney, A. Dunsworth, E. Farhi, B. Foxen, A. Fowler, C. Gidney, M. Giustina, R. Graff, K. Guerin, S. Habegger, M. P. Harrigan, M. J. Hartmann, A. Ho, M. Hoffmann, T. Huang, T. S. Humble, S. V. Isakov, E. Jeffrey, Z. Jiang, D. Kafri, K. Kechedzhi, J. Kelly, P. V. Klimov, S. Knysh, A. Korotkov, F. Kostritsa, D. Landhuis, M. Lindmark, E. Lucero, D. Lyakh, S. Mandrà, J. R. Mc-Clean, M. McEwen, A. Megrant, X. Mi, K. Michielsen, M. Mohseni, J. Mutus, O. Naaman, M. Neeley, C. Neill, M. Y. Niu, E. Ostby, A. Petukhov, J. C. Platt, C. Quintana, E. G. Rieffel, P. Roushan, N. C. Rubin, D. Sank, K. J. Satzinger, V. Smelyanskiy, K. J. Sung, M. D. Trevithick, A. Vainsencher, B. Villalonga, T. White, Z. J. Yao, P. Yeh, A. Zalcman, H. Neven, and J. M. Martinis, Quantum supremacy using a programmable superconducting processor, Nature **574**, 505–510 (2019).
- [19] H.-S. Zhong, H. Wang, Y.-H. Deng, M.-C. Chen, L.-C. Peng, Y.-H. Luo, J. Qin, D. Wu, X. Ding, Y. Hu, P. Hu, X.-Y. Yang, W.-J. Zhang, H. Li, Y. Li, X. Jiang, L. Gan, G. Yang, L. You, Z. Wang, L. Li, N.-L. Liu, C.-Y. Lu, and J.-W. Pan, Quantum computational advantage using photons, Science 370, 1460–1463 (2020).
- [20] L. S. Madsen, F. Laudenbach, M. F. Askarani, F. Rortais, T. Vincent, J. F. F. Bulmer, F. M. Miatto, L. Neuhaus, L. G. Helt, M. J. Collins, A. E. Lita, T. Gerrits, S. W. Nam, V. D. Vaidya, M. Menotti, I. Dhand, Z. Vernon, N. Quesada, and J. Lavoie, Quantum computational advantage with a programmable photonic processor, Nature (London) 606, 75 (2022).
- [21] B. Collins, Moments and cumulants of polynomial random variables on unitary groups, the itzykson-zuber integral and free probability, International Mathematics Research Notices 2003 (2002).
- [22] M. L. Mehta, Random Matrices, 3rd ed., Pure and Applied Mathematics, Vol. 142 (Academic Press, San Diego, 2004).
- [23] B. Collins and P. Śniady, Integration with respect to the haar measure on unitary, orthogonal and symplectic group, Communications in Mathematical Physics 264, 773–795 (2006).
- [24] G. W. Anderson, A. Guionnet, and O. Zeitouni, An Introduction to Random Matrices, Cambridge Studies in Advanced Mathematics (Cambridge University Press, Cambridge, 2009).
- [25] T. Tao, Topics in Random Matrix Theory, Graduate Studies in Mathematics, Vol. 132 (American Mathematical Society, Providence, RI, 2012).
- [26] E. Knill, Approximation by quantum circuits (1995), arXiv:quant-ph/9508006 [quant-ph].
- [27] J. Emerson, Y. S. Weinstein, M. Saraceno, S. Lloyd, and D. G. Cory, Pseudo-random unitary operators for quantum information processing, Science 302, 2098 (2003).
- [28] C. Dankert, Efficient simulation of random quantum states and operators (2005), arXiv:quant-ph/0512217

- [quant-ph].
- [29] D. Gross, K. Audenaert, and J. Eisert, Evenly distributed unitaries: On the structure of unitary designs, Journal of Mathematical Physics 48, 10.1063/1.2716992 (2007).
- [30] A. Ambainis and J. Emerson, Quantum t-designs: t-wise independence in the quantum world (2007), arXiv:quantph/0701126 [quant-ph].
- [31] A. Roy and A. J. Scott, Unitary designs and codes, Designs, Codes and Cryptography 53, 13–31 (2009).
- [32] C. Dankert, R. Cleve, J. Emerson, and E. Livine, Exact and approximate unitary 2-designs and their application to fidelity estimation, Phys. Rev. A 80, 012304 (2009).
- [33] A. A. Mele, Introduction to haar measure tools in quantum information: A beginner& apos; s tutorial, Quantum 8, 1340 (2024).
- [34] J. Emerson, Y. S. Weinstein, M. Saraceno, S. Lloyd, and D. G. Cory, Pseudo-random unitary operators for quantum information processing, Science 302, 2098 (2003).
- [35] C. Dankert, R. Cleve, J. Emerson, and E. Livine, Exact and approximate unitary 2-designs and their application to fidelity estimation, Physical Review A 80, 012304 (2009), arXiv:quant-ph/0606161.
- [36] F. G. Brandão, A. W. Harrow, and M. Horodecki, Efficient quantum pseudorandomness, Physical Review Letters 116, 10.1103/physrevlett.116.170502 (2016).
- [37] F. G. S. L. Brandão, A. W. Harrow, and M. Horodecki, Local random quantum circuits are approximate polynomial-designs, Communications in Mathematical Physics 346, 397–434 (2016).
- [38] F. G. Brandão, W. Chemissany, N. Hunter-Jones, R. Kueng, and J. Preskill, Models of quantum complexity growth, PRX Quantum 2, 10.1103/prxquantum.2.030316 (2021).
- [39] T. Schuster, J. Haferkamp, and H.-Y. Huang, Random unitaries in extremely low depth, Science 389, adv8590 (2025), arXiv:2407.07754 [quant-ph].
- [40] A. W. Harrow and R. A. Low, Random quantum circuits are approximate 2-designs, Communications in Mathematical Physics 291, 257–302 (2009).
- [41] Y. Nakata, C. Hirche, M. Koashi, and A. Winter, Efficient quantum pseudorandomness with nearly time-independent hamiltonian dynamics, Phys. Rev. X 7, 021006 (2017).
- [42] E. Onorati, O. Buerschaper, M. Kliesch, W. Brown, A. H. Werner, and J. Eisert, Mixing properties of stochastic quantum hamiltonians, Communications in Mathematical Physics **355**, 905–947 (2017).
- [43] A. Bhattacharyya, W. Chemissany, S. S. Haque, and B. Yan, Towards the web of quantum chaos diagnostics, The European Physical Journal C 82, 10.1140/epjc/s10052-022-10035-3 (2022).
- [44] M. Fava, J. Kurchan, and S. Pappalardi, Designs via free probability, Phys. Rev. X 15, 011031 (2025).
- [45] S. Guo, M. Sasieta, and B. Swingle, Complexity is not enough for randomness, SciPost Physics 17, 10.21468/scipostphys.17.6.151 (2024).
- [46] L. Cui, T. Schuster, L. Mao, H.-Y. Huang, and F. Brandao, Random unitaries from hamiltonian dynamics (2025), arXiv:2510.08434 [quant-ph].
- [47] S.-K. Jian, G. S. Bentsen, and B. Swingle, Linear growth of circuit complexity from brownian dynamics, Journal of High Energy Physics 2023 (2022).
- [48] A. Tiutiakina, A. D. Luca, and J. de Nardis, Frame potential of brownian syk model of majorana and dirac

- fermions, Journal of High Energy Physics 2024, 1 (2023).
- [49] B. Vermersch, A. Elben, M. Dalmonte, J. I. Cirac, and P. Zoller, Unitary k-designs via random quenches in atomic hubbard and spin models: Application to the measurement of rényi entropies, Physical Review A 97, 10.1103/physreva.97.023604 (2018).
- [50] J. Edwards and D. Thouless, Numerical studies of localization in disordered systems, Journal of Physics C: Solid State Physics 5, 807 (2001).
- [51] D. J. Thouless, Electrons in disordered systems and the theory of localization, Physics Reports 13, 93 (1974).
- [52] C. W. J. Beenakker, Random-matrix theory of quantum transport, Rev. Mod. Phys. 69, 731 (1997).
- [53] E. Akkermans and G. Montambaux, Mesoscopic Physics of Electrons and Photons (Cambridge University Press, 2007).
- [54] F. Evers and A. D. Mirlin, Anderson transitions, Rev. Mod. Phys. 80, 1355 (2008).
- [55] A. Chan, A. De Luca, and J. T. Chalker, Spectral statistics in spatially extended chaotic quantum many-body systems, Phys. Rev. Lett. 121, 060601 (2018).
- [56] J. J. Benedetto and M. Fickus, Finite normalized tight frames, Advances in Computational Mathematics 18, 357 (2003).
- [57] A. Roy and A. J. Scott, Weighted complex projective 2-designs from bases: Optimal state determination by orthogonal measurements, Journal of Mathematical Physics 48, 072110 (2007), arXiv:quant-ph/0703025.
- [58] P. G. Casazza and G. Kutyniok, eds., Finite Frames: Theory and Applications, Applied and Numerical Harmonic Analysis (Birkhäuser, New York, 2012).
- [59] S. Sachdev and J. Ye, Gapless spin-fluid ground state in a random quantum heisenberg magnet, Physical Review Letters 70, 3339 (1993), arXiv:cond-mat/9212030.
- [60] A. Kitaev, A simple model of quantum holography, Talks at KITP, University of California, Santa Barbara (2015), accessed 2025-10-16.
- [61] J. Polchinski and V. Rosenhaus, The spectrum in the sachdev-ye-kitaev model, Journal of High Energy Physics 2016, 001 (2016), arXiv:1601.06768.
- [62] J. Maldacena and D. Stanford, Remarks on the sachdev—ye–kitaev model, Physical Review D 94, 106002 (2016), arXiv:1604.07818.
- [63] J. Maldacena, D. Stanford, and Z. Yang, Conformal symmetry and its breaking in two-dimensional nearly anti-de sitter space, Progress of Theoretical and Experimental Physics 2016, 12C104 (2016), arXiv:1606.01857.
- [64] A. Kitaev and S. J. Suh, The soft mode in the sachdev—ye–kitaev model and its gravity dual, Journal of High Energy Physics 2018, 183 (2018), arXiv:1711.08467.
- [65] D. Bagrets, A. Altland, and A. Kamenev, Sachdev-ye-kitaev model as liouville quantum mechanics, Nuclear Physics B 911, 191 (2016), arXiv:1607.00694.
- [66] D. Bagrets, A. Altland, and A. Kamenev, Power-law outof-time-order correlation functions in the syk model, Nuclear Physics B 921, 727 (2017), arXiv:1702.08902.
- [67] A. Jevicki, K. Suzuki, and J. Yoon, Bi-local holography in the syk model, Journal of High Energy Physics 2016, 007 (2016), arXiv:1603.06246.
- [68] A. M. García-García and J. J. M. Verbaarschot, Spectral and thermodynamic properties of the sachdev-ye-kitaev model, Physical Review D 94, 126010 (2016), arXiv:1610.03816.

- [69] A. M. García-García and J. J. M. Verbaarschot, Analytical spectral density of the sachdev-ye-kitaev model at finite n, Physical Review D 96, 066012 (2017), arXiv:1701.06593.
- [70] Y. Gu, X.-L. Qi, and D. Stanford, Local criticality, diffusion and chaos in generalized sachdev-ye-kitaev models, Journal of High Energy Physics 2017, 125 (2017), arXiv:1609.07832.
- [71] X.-Y. Song, C.-M. Jian, and L. Balents, Strongly correlated metal built from sachdev-ye-kitaev models, Physical Review Letters 119, 216601 (2017), arXiv:1705.00117.
- [72] V. Rosenhaus, An introduction to the syk model, Journal of Physics A: Mathematical and Theoretical 52, 323001 (2019), arXiv:1807.03334.
- [73] D. Chowdhury, A. Georges, O. Parcollet, and S. Sachdev, Sachdev-ye-kitaev models and beyond: A window into non-fermi liquids, Reviews of Modern Physics 94, 035004 (2022), arXiv:2109.05037.
- [74] There are two contributors to the uncertainty: (i) finite-sampling noise from a limited number of disorder realizations, and (ii) oscillations of the averaged SFF near the Thouless time.
- [75] A. Altland and D. Bagrets, Quantum ergodicity in the SYK model, Nucl. Phys. B 930, 45 (2018), arXiv:1712.05073 [cond-mat.str-el].
- [76] A. Altland, D. Bagrets, P. Nayak, J. Sonner, and M. Vielma, From operator statistics to wormholes, Phys. Rev. Res. 3, 033259 (2021), arXiv:2105.12129 [hep-th].
- [77] The model has been argued to have a Thouless time of order  $\log N$  in [93].
- [78] Y. Sekino and L. Susskind, Fast scramblers, Journal of High Energy Physics 2008, 065–065 (2008).
- [79] Although the complex SYK<sub>2</sub> model does not realize a k-design, it still reaches the Brownian value also for higher orders k; see SM [80] for details.
- [80] See the Supplemental Material (SM) for details: (A) a detailed computation of the frame potential (FP) for the multiple-quench protocol; (B) a step-by-step derivation of the first-order FP for single-quench evolution generated by GUE Hamiltonians; (C) additional numerics for single-quench FP in integrable models (the free SYK<sub>2</sub> and interacting Richardson models); (D) additional numerical results for single-quench dynamics in chaotic models; and (E) a brief overview of analytic results for the complex Brownian SYK model.
- [81] M. B. Hastings and A. W. Harrow, Classical and quantum tensor product expanders, Quantum Information & Computation 9, 336 (2009), arXiv:0804.0011 [quant-ph].
- [82] A. W. Harrow and R. A. Low, Efficient quantum tensor product expanders and k-designs, in Approximation,

- Randomization, and Combinatorial Optimization. Algorithms and Techniques (APPROX/RANDOM 2009), Lecture Notes in Computer Science, Vol. 5687 (Springer, Berlin, Heidelberg, 2009) pp. 548–561, arXiv:0811.2597 [quant-ph].
- [83] P. Sen, Efficient quantum tensor product expanders and unitary t-designs via the zigzag product (2018), arXiv:1808.10521 [quant-ph].
- [84] D. Gross, K. Audenaert, and J. Eisert, Evenly distributed unitaries: On the structure of unitary designs, Journal of Mathematical Physics 48, 052104 (2007), arXiv:quantph/0611002.
- [85] J. Haferkamp, Random quantum circuits are approximate unitary t-designs in depth  $O(nt^{5+o(1)})$ , Quantum **6**, 795 (2022), arXiv:2203.16571 [quant-ph].
- [86] We illustrate this with the complex SYK model and the GUE random-matrix model; the protocol also extends to other systems, such as the Majorana SYK model (see [80]).
- [87] Y. Nakata, D. Zhao, T. Okuda, E. Bannai, Y. Suzuki, S. Tamiya, K. Heya, Z. Yan, K. Zuo, S. Tamate, Y. Tabuchi, and Y. Nakamura, Quantum circuits for exact unitary t-designs and applications to higher-order randomized benchmarking, PRX Quantum 2, 030339 (2021).
- [88] E. Bannai, Y. Nakata, T. Okuda, and D. Zhao, Explicit construction of exact unitary designs, Advances in Mathematics 405, 108457 (2022).
- [89] T. Schuster, F. Ma, A. Lombardi, F. Brandao, and H.-Y. Huang, Strong random unitaries and fast scrambling (2025), arXiv:2509.26310 [quant-ph].
- [90] R. Baumgartner, P. Pelliconi, S. Bandyopadhyay, F. Orsi, N. Sauerwein, P. Hauke, J.-P. Brantut, and J. Sonner, Quantum simulation of the sachdev-ye-kitaev model using time-dependent disorder in optical cavities (2024), arXiv:2411.17802 [quant-ph].
- [91] P. Uhrich, S. Bandyopadhyay, N. Sauerwein, J. Sonner, J.-P. Brantut, and P. Hauke, A cavity quantum electrodynamics implementation of the sachdev-ye-kitaev model (2023), arXiv:2303.11343 [quant-ph].
- [92] Note that in [48], all charge sectors are summed up, so there is an additional factor of  $N^k$ . We only consider one fixed charge sector.
- [93] H. Gharibyan, M. Hanada, S. H. Shenker, and M. Tezuka, Onset of random matrix behavior in scrambling systems, Journal of High Energy Physics 2018, 10.1007/jhep07(2018)124 (2018).